

CHARACTERIZING MESO-SCALE HETEROGENEITIES IN RESERVOIR ROCKS

Ronny Pini and Sally M. Benson

Department of Energy Resources Engineering, Stanford University, Stanford (USA)

This paper was prepared for presentation at the International Symposium of the Society of Core Analysts held in Napa Valley, California, USA, 16-19 September, 2013

ABSTRACT

Results are presented from a newly developed technique that allows measuring drainage capillary pressure curves during core-flooding experiments; data have been collected for the N_2 /water and $scCO_2$ /brine system. One of the strengths of the proposed technique is that by combination with X-ray CT imaging, capillary pressure-saturation relationships can be obtained for mm-scale subsets of the rock sample; these are of high relevance as they directly and non-destructively quantify small-scale capillary heterogeneity in these systems. Furthermore, the spatial variability of the capillary pressure curve can be represented in terms of a single scaling factor, thus simplifying considerably the description of heterogeneity. The obtained scaling factors are further translated into a corresponding distribution of permeabilities, thus creating a unique and consistent framework where multiphase- and rock-properties are integrated.

INTRODUCTION

Geological formations present heterogeneities at various scales; interestingly enough, mm- to cm-scale features that are commonly observed in sedimentary rocks [1] have been shown to greatly influence fluid transport at these large observational scales (tens to hundreds of meters) [2,3]. The ability of quantifying these processes at a scale where flow is described by continuum-scale physics and where those small-scale heterogeneities are taken into account represents a critical step in the effort of creating a link between the pore- and the reservoir-scale. One way to accomplish this is by adopting an integrated approach that combines displacement experiments in naturally heterogeneous core-samples with the simultaneous imaging of flow as well as with the support of detailed numerical simulations [4]. In this context, x-ray CT scanning has been proven to be very effective in providing both *qualitative* and *quantitative* characterization of porosity and fluid-phase saturations at a resolution of a few mm^3 (a volume that exceeds the size of a porosity-based REV for most sandstones) at any time during a core-flooding experiment [5]. Most importantly, experimental protocols were developed that independently validate the existence of spatially varying capillary pressure curves at the sub-core scale [6]. As a matter of fact, numerical simulations fail to reproduce sub-core scale saturation distributions observed during core-flooding experiments when a single capillary pressure curve is applied, and appropriate scaling laws for the capillary pressure need to be incorporated [4]. Built on this knowledge, a methodology is presented here that allows

for the characterization of meso-scale heterogeneities within a laboratory sample based solely on experimental observations. Spatially distributed capillary pressure curves are measured at a scale of $\sim 4 \text{ mm}^3$ in a Berea Sandstone core; it is shown that capillary heterogeneity is significant and that it can be represented in terms of a single scaling factor, thus simplifying considerably the description of heterogeneity. Additionally, upon precise visualization of fluid saturations and porosity distributions, the obtained scaling factors are translated into a corresponding distribution of permeabilities, thus creating a unique and consistent framework where multiphase- and rock-properties are integrated.

METHODS AND MATERIALS

Capillary Pressure Measurements

The technique to obtain a drainage capillary pressure curve during a core-flooding experiment is explained in a previous publication [6]. Briefly, a nonwetting phase (in this study N_2 or CO_2) is injected at constant flow rate, q_{inj} , into the core to displace a wetting phase (water or brine) until steady-state conditions are attained, i.e. when water production stops and its pressure within the core reaches a constant level. Accordingly, viscous and capillary pressure gradients within the core are identical, and the capillary pressure at its inlet face ($x = 0$) corresponds to the measured pressure drop, ΔP ,

$$\Delta P = P_1 - P_2 = P_c|_{x=0} \quad (1)$$

where $P_1 = P_{\text{nw}}(x = 0)$ and $P_2 = P_w(x = 0) = P_w(x = L)$ are measured in the end-caps mounted just outside of the inlet and outlet faces of the core. By performing experiments at increasing injection rates, increasingly higher capillary pressures can be attained; the latter can be related to saturations measured at the inlet face of the core and a capillary pressure curve can therefore be constructed. One of the benefits of the method described in [6] resides in the use of x-ray CT scanning to observe and quantify fluid saturations in a rock core, thus allowing for the measurement of capillary pressure curves at various positions and spatial scales within the sample. In fact, the functional relationship between capillary pressure and saturation is obtained for the inlet slice of the rock using the average saturation and capillary pressure measured there, and sub-core scale capillary pressure curves are constructed by linking the measured capillary pressure value to the saturation observed in each subset (voxel) of same slice.

Scaling of the Capillary Pressure Curve

With the aim of simplifying the description of the statistical variability of a spatially distributed property such as the capillary pressure, hydrologists have often adopted a scaling approach [7]. The latter makes use of so-called scaling factors α_j to relate the capillary pressure at a given location, $P_{c,j}$, to a representative mean, \hat{P}_c , i.e.

$$P_{c,j}(S) = \frac{1}{\alpha_j} \hat{P}_c(S) \quad j = 1, \dots, N_{\text{vox}} \quad (2)$$

For the present study, the experimental data set consists of N_{vox} locations (voxels), N_{pc} capillary pressure values (or flow rates) and $N_{\text{vox}} \times N_{\text{pc}}$ saturation values. The scaling factors for each voxel are found by minimizing the following objective function,

$$F = \prod_{j=1}^{N_{\text{vox}}} \prod_{k=1}^{N_{\text{pc}}} \frac{1}{a_j} P_{c,j}(S_{j,k}) - \hat{P}_c(S_{j,k}) \hat{u}_j^2 \quad (3)$$

In this study, the representative capillary pressure function, $\hat{P}_c(S)$, is the one obtained by considering the entire inlet slice of the core (average saturation). Given that the volume of a single slice is about 2 cm^3 (i.e. similar to the typical volume used for mercury intrusion experiments) and that the Berea Sandstone core considered in this study is relatively homogeneous, the obtained curve is assumed to be representative for the entire core. Spatial variations in a multiphase flow property, such as the capillary pressure, are essentially driven by variations in properties of the rock, such as porosity and permeability [8]. These can be linked together through the well-known J -Leverett function, $J(S)$, a scaling law of the same form as Eq.(2) [9],

$$J(S) = \frac{P_c(S)}{\gamma_{12}} \sqrt{\frac{k}{e}} \quad (4)$$

where γ_{12} is the interfacial tension of the given fluid pair, while ε and k are the rock's porosity and permeability, respectively. While in its original form this function was intended to scale data among lithologically similar core samples [10], a number of investigators have subsequently applied it to capture capillary heterogeneity at the sub-core scale [4,8]. This last approach is followed here and allows obtaining an expression for the scaling factor a_j as a function of porosity and permeability. In fact, equating Eq.(4) applied to the core and to a given voxel j , and combining with Eq.(2) gives

$$a_j = \sqrt{\frac{k_j / e_j}{\hat{k} / \hat{e}}} \quad (5)$$

In other words, permeability heterogeneity at the sub-core scale can be readily quantified, once the core's average porosity and permeability, as well as the distribution of porosities and scaling factors are known.

Rock, Fluids and Experimental Procedure

Rocks. A 8.5 cm-long, 5 cm-diameter Berea Sandstone core, fired at 700°C , was used. Its permeability to water is 325 mD and its porosity (18.8%) was measured by x-ray CT scanning as described in [6]. Two additional analyses were performed on a small plug (diameter 6 mm, length 10 mm) that was drilled from a section adjacent to the inlet face of the core, namely Helium pycnometry (AccuPyc II 1340, Micromeritics) to estimate the skeletal density of the rock ($\rho_{\text{sk}}=2.644 \text{ g/cm}^3$), and mercury intrusion porosimetry (Micromeritics Autopore IV) to obtain a capillary pressure curve (MICP). The latter was

corrected upon application of the Helium skeletal density and of an entry pressure of 53.5 kPa, so as to match the rock's porosity measured by x-ray CT scanning.

Fluids. CO₂ and N₂ (both with a purity of 99.9%, Praxair, Inc.), tap water and brine (NaCl:KCl / 0.864:0.136, total salt molality 2.5 mol/kg) were used in the core flooding experiments. At the experimental conditions of the core-flood, the interfacial tension γ_{12} of the N₂/Water (50°C and 2.4 MPa) and of the CO₂/brine (50°C and 9 MPa) systems take values of 65 and 41 mN/m, respectively, while for the Mercury/Air system (MICP data) $\gamma_{HgA}=485$ mN/m and $\theta_{HgA}=40^\circ$, the latter representing the contact angle in the wetting phase. Note that the relationship proposed by [12] is used to convert the MICP data to any given fluid pair by using the contact angle θ_{12} as a fitting parameter.

Procedure. A detailed description of both the apparatus and the experimental procedure is reported in a previous publication [11]. The latter is used to purge the system of air, pre-equilibrate the nonwetting and wetting fluid phases with each other at experimental conditions, and take background scans. For the capillary pressure experiments, a total of 10 PV are allowed to circulate through the core at each selected flow rate in order to ensure that steady-state conditions are achieved, followed by the acquisition of a scan (imaging parameters: voxel dimension (0.5×0.5×1)mm³, tube current 200 mA, energy level of the radiation 120 keV, display field of view 25 cm). The image that is obtained upon averaging among 15 scans taken at the exact same location is further processed by applying a (2×2×1)mm³ coarsening scheme, thus reducing the uncertainty associated to the computed porosity and saturation values at the voxel scale to 0.3%abs. and 2%abs., respectively [6]. Note this voxel volume is well above the REV typically considered for sandstones and it can therefore be associated to continuum scale properties, such as porosity, permeability and saturations.

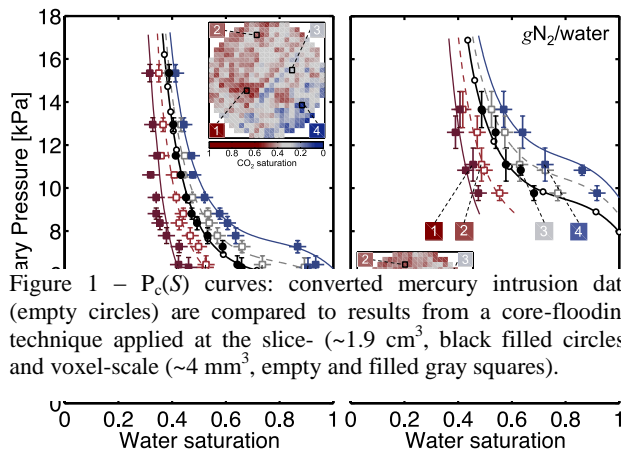


Figure 1 – $P_c(S)$ curves: converted mercury intrusion data (empty circles) are compared to results from a core-flooding technique applied at the slice- (~1.9 cm³, black filled circles) and voxel-scale (~4 mm³, empty and filled gray squares).

the slice; these are indicated by the 2D saturation map shown in the inset of the figure and are characterized by an early or late invasion of the nonwetting phase as compared to the average slice saturation.

RESULTS AND DISCUSSION

Figure 1 shows core- (circles) and voxel-scale (squares) capillary pressure curves as obtained upon plotting the pressure drop across the core as a function of the slice- and voxel-saturations observed at the inlet face of the core, respectively. For the sake of better visualization, in the latter case only four curves are plotted that represent four distinct positions in

Results are also shown from an independent mercury intrusion experiment (empty circles) carried out on a small plug and that have been converted to the given fluid pair upon using the contact angle as a fitting parameter ($\theta_{12} = 38.8^\circ$ and 39.2° for N_2 /water and CO_2 /brine, respectively). The agreement between the two techniques is very good and the obtained contact angle suggests that strong wetting conditions prevail, its value being almost identical to the one imposed for the mercury/air system. Additionally, at a given capillary pressure level, the four mm-scale capillary pressure curves are shifted towards higher or lower saturation values, but retain a similar shape as the mean curve; this is evidenced by the colored lines in the figure that are drawn primarily to guide the eye, but that result merely from a shift of the mercury data toward higher or lower capillary pressure levels.

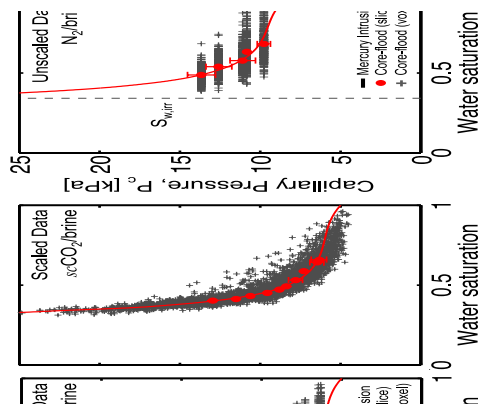
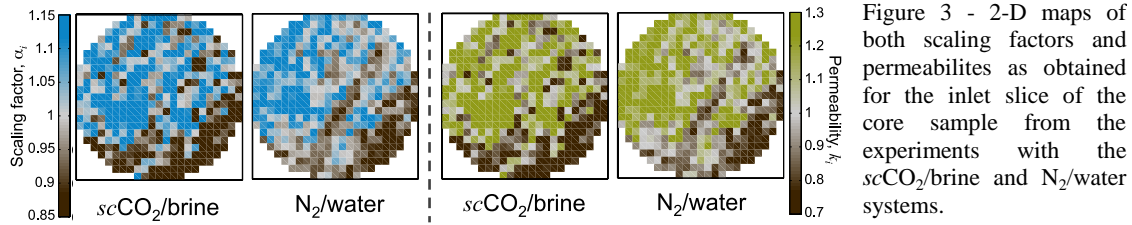


Figure 2 –Unscaled vs. scaled $P_c(S)$ curves for the $scCO_2$ /brine and N_2 /water experiments; circles are results the core-flooding experiments and represent the mean curve against which observations at the voxel scale (plus gray symbols) are scaled. To this aim, mercury and core-flooding data have been interpolated by a spline function (black line).

Unscaled capillary pressure values, $P_{c,j}$, from 413 locations within the inlet slice of the rock sample are shown in Figure 2 for the experiments carried out with the $scCO_2$ /brine (left) and N_2 /water (right) systems, respectively. In the figure, the solid line (a spline interpolation through the inlet-slice capillary pressure data) represents the characteristic capillary pressure curve, while the plus symbols are the (voxel) unscaled data. The same data, now scaled by minimizing Eq.(3), are also shown in Figure 2; it can be seen that the originally scattered data now coalesce nicely into a relatively narrow band around the characteristic capillary pressure curve. The effectiveness of the scaling is reflected in the value of the sum of squares Φ , which is reduced to only about 25% of the value for the unscaled data. In other words, an approach based on constant (location dependent) scaling factors is able to capture the variability of the $P_c(S)$ curve at the sub-core scale, further implying that the description of capillary heterogeneity can be simplified considerably.

The variability of the capillary pressure can be easily visualized from the 2-D maps of the scaling factors shown in Figure 3. It can be seen that the deviations from unity are significant ($\pm 15\%$): values larger than one (blue color) are found for those voxels that require a lower capillary pressure to reach the same saturation as the mean, while the opposite is true for $\alpha < 1$ (brown color).



Most importantly, the two maps, obtained from two independent experiments, are very similar; this is crucial, since capillary heterogeneity ultimately relates to the variation of properties that are directly associated to the microscopic pore structure of the rock. In fact, as given by Eq.(5), permeabilities at the voxel scale can now be computed based solely on the experimental observations, i.e. by combining the derived scaling factors with measured core-averaged porosity and permeability, as well as with the porosity distribution at the voxel scale (from the x-ray images). The resulting 2-D maps are also given in Figure 3; again, the two maps show very similar results, thus confirming the robustness of this technique. It is not surprising that the exact same features appear as for the distribution of the scaling factors, and that deviations from the mean are now larger ($\pm 30\%$).

REFERENCES

1. Murphy, W., J. Roberts, D. Yale, and K. Winkler (1984), *Geophys. Res. Lett.*, 11(8), 697–700.
2. Ringrose, P., K. Sorbie, P. Corbett, and J. Jensen (1993), *J. Pet. Sci. Eng.*, 9(2), 103–124.
3. Ronayne, M. J., S. M. Gorelick, and C. Zheng (2010), *Water Resour. Res.*, 46(10), W10, 519.
4. Krause, M., S. Krevor, and S. M. Benson (2013), *Transp. Porous Media*, pp. in press.
5. Akin, S., and A. R. Kavscek (2003), in *Applications of X-ray Computed Tomography in the Geosciences*, vol. 215, edited by F. Mees, R. Swennen, M. Van Geet, and P. Jacobs, pp. 23–38, Geological Society, London.
6. Pini, R., S. C. M. Krevor, and S. M. Benson (2012), *Adv. Water Res.*, 38, 48-59.
7. Warrick, A., G. Mullen, and D. Nielsen (1977), *Water Resour. Res.*, 13(2), 355–362.
8. Chaouche, M., N. Rakotomalala, D. Salin, B. Xu, and Y. Yortsos (1994), *Chem. Eng. Sci.*, 49(15), 2447–2466.
9. Leverett, M. C. (1941), *T. Soc. Petrol. En. AIME*, 142, 152–169.
10. Brown, H. W. (1951), *T. Soc. Petrol. En. AIME*, 192, 67–74.
11. Pini, R. and S. M. Benson (2013), *Water Resour. Res.*, in press.
12. Purcell, W. R. (1949), *J. Pet. Technol.*, 1(2), 39–48.